POLYOXOMETALATES

Open Access
RESEARCH ARTICLE

Sandwich-type thorium-substituted phosphotungstate for the catalytic synthesis of aza-heterocycles

Xuejiao Chen[§], Fuhua Zhang[§], Jiawei Cao, Zhibin Zhang[✉], and Guoping Yang[✉]

Jiangxi Key Laboratory for Mass Spectrometry and Instrumentation, School of Chemistry and Materials Science, East China University of Technology, Nanchang 330013, China
[§]Xuejiao Chen and Fuhua Zhang contributed equally to this work.

Cite This: *Polyoxometalates*, **2026**, *5*, 9140121

Read Online

ABSTRACT: A novel sandwich-type thorium-substituted phosphotungstate, $[H_2N(CH_3)_2]_{10}[Th(PW_{11}O_{39})_2]\cdot 24H_2O$ (**ThP_2W_{22}**), was synthesized and fully characterized. The structure consists of two monolacunary Keggin-type $[PW_{11}O_{39}]^{7-}$ units bridged by an eight-coordinate Th^{4+} center. **ThP_2W_{22}** functions as an efficient Lewis acid catalyst for the synthesis of 2,3-dihydroquinazolinones via cyclization of 2-aminobenzamides with aldehydes. A series of quinazolinone derivatives was obtained in high yields (75%–92%) under mild and green reaction conditions. Control experiments indicate a synergistic interaction between the Th^{4+} center and the polyoxometalate framework, highlighting the potential of thorium-containing polyoxometalates as catalysts for heterocycle synthesis.

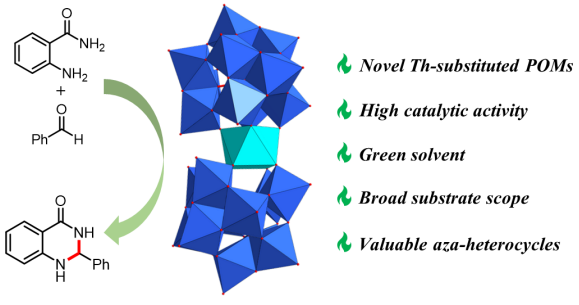

KEYWORDS: polyoxometalates, thorium, catalysis, aza-heterocycles

1 Introduction

In heteropolyoxometalate systems, lacunary polyoxometalates (POMs) act as versatile building blocks with strong affinity and coordination capacity toward metal ions due to their high coordination reactivity [1–3]. This property has been widely exploited for the directional modification of metal centers [4–8]. In recent years, research has primarily focused on doping with transition and lanthanide metals, leading to significant advances in structural regulation, performance optimization, and application development [9–14]. In contrast, actinide-containing POMs remain largely unexplored, and their structural design principles, coordination mechanisms, and structure–property relationships have not been systematically established [15–20]. Incorporation of thorium (Th) into lacunary POM frameworks can enrich structural diversity and provide a model platform for investigating the unique electronic structures, coordination behavior, and bonding characteristics of actinides.

As a high-valent actinide ion, Th^{4+} possesses a large ionic radius and high charge density. Its strong electric field significantly polarizes coordinated water molecules, thereby promoting hydrolysis and generating various hydrolyzed species [21–24]. These species are generally unstable and undergo successive stepwise hydrolysis, forming a series of mononuclear hydroxo complexes, such as $Th(OH)_2^{2+}$, which can substantially affect the chemical system [23, 25–28]. Furthermore, incorporating Th^{4+} into POM frameworks with the coordination geometries is typically observed in POM chemistry remains challenging. To date, only seven types of Th-containing POMs have been reported, including tungstate-based structures with classical Keggin, Dawson, Weakley, and Silverton configurations [29–32]. Previous studies have shown that Keggin-type POM frameworks can accommodate multiple thorium ions. Loiseau and co-workers reported a Th-containing arsenotungstate, $[K_4\{Th_3(H_2O)_3\{AsO(\mu_2\text{-}O)_3\}_2\}\{Th_3(H_2O)_2\{AsO(\mu_2\text{-}O)_3\}_2\}_3(AsW_{10}O_{38})_6]^{38-}$ [33], which contains twelve Th ions encapsulated by six lacunary Keggin-type POM units and represents the largest Th-containing POM reported to date. In contrast, when phosphorus—an element in the same group as arsenic—is employed as the heteroatom, Th-containing phosphotungstates exhibit limited structural diversity, and their catalytic potential remains largely unexplored. Therefore, the development of novel synthetic strategies for Th-containing phosphotungstates and systematic evaluation of their catalytic properties are of considerable research significance.

In this study, a novel sandwich-type Th-containing phosphotungstate, $[H_2N(CH_3)_2]_{10}[Th(PW_{11}O_{39})_2]\cdot 24H_2O$ (**ThP_2W_{22}**), was synthesized from simple starting materials and fully characterized. The compound comprises two monolacunary Keggin-type $[PW_{11}O_{39}]^{7-}$ anions coordinated to a single eight-coordinate Th^{4+} center. The resulting complex crystallizes in the $P2_1/c$ space group and adopts a layered packing arrangement. Successful incorporation of Th^{4+} into the phosphotungstate

Received: December 12, 2025; **Revised:** January 20, 2026
Accepted: February 4, 2026

✉Address correspondence to Zhibin Zhang, zhbzhang@ecut.edu.cn; Guoping Yang, erick@ecut.edu.cn

https://doi.org/10.26599/POM.2026.9140121

framework affords a well-defined sandwich-type structure, effectively mitigating the challenges associated with thorium hydrolysis and coordination instability. Furthermore, this work demonstrates, for the first time, the application of Th-containing POMs as efficient Lewis acid catalysts for the synthesis of pharmacologically relevant aza-heterocycles. **ThP_2W_{22}** exhibits excellent catalytic performance in the condensation of aldehydes with 2-aminobenzamides, affording a series of 2,3-dihydroquinazolinones in yields of up to 94% under mild and green reaction conditions.

2 Experimental

2.1 Synthesis of ThP_2W_{22}

$Na_2WO_4{\cdot}2H_2O$ (6.00 mmol, 1.98 g), $(CH_3)_2NH_2Cl$ (12.0 mmol, 0.979 g), $Na_2HPO_4{\cdot}12H_2O$ (0.600 mmol, 0.215 g), KCl (0.800 mmol, 0.321 g), and squaric acid (0.300 mmol, 0.0340 g) were sequentially dissolved in 1 M NaAc/HAc buffer (pH 4.8) and stirred for 5 min until a clear solution was obtained. The pH was adjusted to 4.5 with dilute HCl and the mixture was stirred for an additional 10 min. $ThCl_4{\cdot}6H_2O$ (0.600 mmol, 0.224 g) was then added, and after complete dissolution, the pH was further adjusted to 4.0. The resulting yellow solution was heated at 85 °C with stirring for 40 min. After cooling to room temperature, the solution was filtered and allowed to stand at room temperature. Colorless rod-shaped crystals formed after one week (yield: 31.2%, based on Th). FT-IR (cm^{-1}): 3564 (m), 3133 (m), 1570 (m), 1043 (w), 946 (s), 883 (vs), 719 (vs), 685 (vs).

2.2 Typical procedure for Aza-heterocycle synthesis

In a 4-mL reaction vial, 2-aminobenzamide (1, 0.2 mmol), aldehyde (2, 0.2 mmol), ThP_2W_{22} (0.3 mol%), and EtOH (1 mL) were combined. The sealed screw-cap vial equipped with a Teflon liner was heated at 90 °C for 6 h. After cooling to room temperature, the reaction mixture was purified by column chromatography (petroleum ether/EtOAc) to afford the desired products.

3 Results and discussion

3.1 Structure description

The crystallographic data for **ThP_2W_{22}** are summarized in Table S1 in the Electronic Supplementary Material (ESM). The structural formula, $[H_2N(CH_3)_2]_{10}[Th(PW_{11}O_{39})_2]{\cdot}24H_2O$, was determined from thermogravimetric analysis (Fig. S1 in the ESM). Powder X-ray diffraction (PXRD) patterns show excellent agreement between the experimental and simulated data, confirming the phase purity of **ThP_2W_{22}**. Single-crystal X-ray diffraction analysis indicates that **ThP_2W_{22}** crystallizes in the $P2_1/c$ space group. Bond valence sum calculations confirm oxidation states of +5 for P, +6 for W, and +4 for Th. From a selected orientation, the asymmetric unit exhibits a sandwich-type architecture composed of two monolacunary Keggin-type $[PW_{11}O_{39}]^{7-}$ polyanions coordinated to a central Th^{4+} ion. Each monolacunary $[PW_{11}O_{39}]^{7-}$ unit provides four exposed oxygen donor sites (Fig. 1(a)), which coordinate to the Th^{4+} center to form the complete **ThP_2W_{22}** structure (Fig. 1(b)). Figure 1(c) illustrates the coordination environment of Th, in which the Th^{4+} ion is linked to the $[PW_{11}O_{39}]^{7-}$ units through W–O–Th bridges. The coordinating μ_2-O atoms (O24, O41, O44, O45, O48, O52, O56, and O73) are highlighted in lavender, with Th–O bond lengths ranging from 2.365(1) to 2.505(2) Å. To clarify the spatial packing arrangement, the **ThP_2W_{22}** structure was simplified into a V-shaped ball-and-stick model using the phosphorus and thorium atoms as reference centers (Fig. 1(d)).

The supramolecular structure of **ThP_2W_{22}** (Fig. 1(e)), shown without counterions for clarity, exhibits a three-dimensional layered stacking architecture stabilized by hydrogen bonding interactions (Table S4 in the ESM). Upon rotation of the single-layer stacking diagram, a columnar arrangement becomes evident (Fig. 1(f)), with the columns extending parallel to the *b*-axis. The single-layer architecture is constructed through hydrogen bonds involving N2–H2A···O43, N2–H2A···O26, N2–H2A···O29, and C6–H6B···O7. As illustrated in Fig. 1(g), each layer can be simplified into a model in which adjacent columns adopt opposite orientations, generating an alternating ABAB stacking pattern. Specifically, the V-shaped opening of column A is oriented opposite to the positive *b*-axis direction, whereas column B is aligned along the positive *b*-axis (Fig. 1(h)).

3.2 Catalytic performance

2,3-Dihydroquinazolinones are important aza-heterocycles found in natural products and synthetic compounds, exhibiting diverse pharmacological activities, including antibacterial, antitumor, analgesic, and vasodilatory effects [34–36]. Owing to its operational simplicity and high efficiency, the Lewis acid-catalyzed condensation of 2-aminobenzamides with aldehydes has attracted considerable attention [37–40]. Considering the Lewis acidity of the thorium center and the electronic properties of the substrates, the catalytic performance of **ThP_2W_{22}** was evaluated in the synthesis of 2,3-dihydroquinazolinones via condensation of 2-aminobenzamides with aldehydes.

The catalytic performance of **ThP_2W_{22}** was initially evaluated using the model reaction between 2-aminobenzamide (**1a**, 0.2 mmol) and benzaldehyde (**2a**, 0.2 mmol) to afford 2,3-dihydroquinazolinone. The optimal conditions were determined by systematically varying the solvent, temperature, and reaction time. As summarized in Table 1, under the initial conditions (MeCN, 70 °C, 2 h), the product was obtained in 49% yield (Table 1, entry 1). Replacement of MeCN with several green solvents identified EtOH as the optimal medium, providing the desired product in 62% yield (Table 1, entries 1–5). Subsequent temperature screening established 90 °C as the optimal reaction temperature (Table 1, entries 6–8). Finally, extending the reaction time based on entry 7 showed that increasing the reaction time to 6 h improved the yield to 94% (Table 1, entries 9–11). Further prolongation of the reaction time did not result in additional yield enhancement. Catalyst loading was further investigated. Reducing the loading to 0.2 mol% resulted in a decreased yield (87%), while increasing the catalyst amount did not provide additional improvement. Therefore, 0.3 mol% was selected as the optimal catalyst loading. Under the optimized conditions—**1a** (0.2 mmol), **2a** (0.2 mmol), **ThP_2W_{22}** (0.3 mol%), EtOH (1 mL), 90 °C, 6 h—the reaction proceeded efficiently. The stability and reusability of **ThP_2W_{22}** were subsequently examined under the optimized conditions. The PXRD patterns recorded before and after catalysis were essentially identical, indicating that the structural integrity of **ThP_2W_{22}** was maintained during the catalytic process (Fig. S3 in the ESM). Recycling experiments showed that **ThP_2W_{22}** retained satisfactory catalytic activity over five consecutive cycles (Fig. S4 in the ESM),

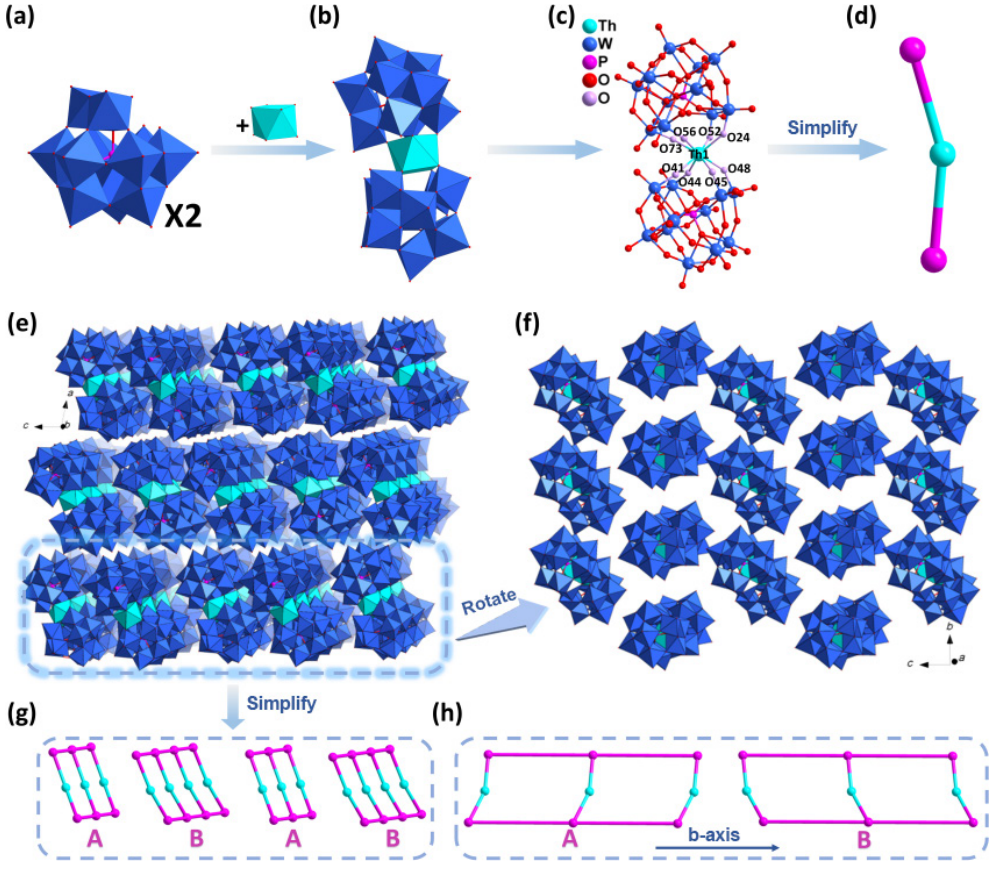

Figure 1 (a) PW_{11} unit. (b) The asymmetric cell structure of **ThP_2W_{22}**. (c) The ball-stick model of **ThP_2W_{22}**. (d) Simplified scheme of the V-shape for **ThP_2W_{22}**. (e) Schematic diagram of the 3D stacking of **ThP_2W_{22}** as viewed along the *b*-axis. (f) Top view of a single-layer stack diagram for *b*-*c* plane. (g) Simplified schematic of a single-layer stacking diagram for *b*-*c* plane. (h) Stacking direction of columns A and B. Color code: P, pink; W, light blue; Th, turquiose; O, red/lavender.

Table 1 Optimization of reaction conditions[a]

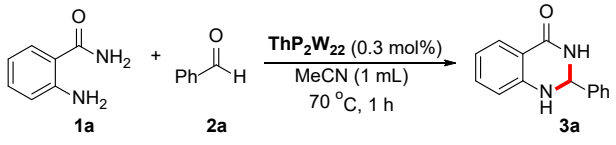

Entry	Solvent	Temperature (°C)	Time (h)	Yield[b] (%)
1	MeCN	70	2	49
2	EtOH	70	2	62
3	PC	70	2	40
4	EA	70	2	38
5	H_2O	70	2	30
6	EtOH	80	2	69
7	EtOH	90	2	81
8	EtOH	100	2	82
9	EtOH	90	4	89
10	EtOH	90	6	94
11	EtOH	90	8	93
12[c]	EtOH	90	6	87
13[d]	EtOH	90	6	92

[a]Reaction conditions: 2-aminobenzamide (**1a**, 0.2 mmol), benzaldehyde (**2a**, 0.2 mmol), solvent (1 mL), **ThP_2W_{22}** (0.3 mol%), 70 °C for 2 h. [b]The yields were determined by gas chromatography (GC) with biphenyl as the internal standard. [c]**ThP_2W_{22}** (0.2 mol%). [d]**ThP_2W_{22}** (0.4 mol%).

further demonstrating its excellent stability and reusability.

Encouraged by the favorable catalytic performance, the substrate scope of the developed system was evaluated for the condensation of 2-aminobenzamides with aldehydes. As summarized in Fig. 2, the influence of substituents on the phenyl ring of substrate **1** was first examined using benzaldehyde (**2a**) as the model aldehyde. Both electron-donating and electron-withdrawing groups exerted only a minor influence on the reaction efficiency, affording products **3a**–**3d** in yields of 83%–92%. The effect of substituents on the amide moiety of **1** was also investigated. Among the tested substrates, 2-amino-*N*-(cyclopropylmethyl)benzamide provided the highest yield (**3h**, 92%), followed by 2-amino-*N*-isopropylbenzamide (**3g**, 91%), 2-amino-*N*-benzylbenzamide (**3f**, 81%), and 2-amino-N-phenylbenzamide (**3e**, 75%). The observed trend is likely attributable to steric effects associated with the *N*-substituents. In addition, benzaldehydes bearing various substituents, including –Me, –OMe, –^{i}Pr, –F, –Cl, and –Br (**3i**–**3p**), were well tolerated, affording the desired products in moderate to good yields. Steric hindrance influenced the reaction outcome, as reflected by the higher yields of **3m** and **3n** compared with **3o**. Overall, aldehydes containing electron-withdrawing groups generally favored the transformation, presumably due to enhanced electrophilicity of the carbonyl group.

Control experiments were performed to elucidate the catalytic mechanism. As shown in Fig. 3(a), both $ThCl_4$ and $Na_9[A\text{-}PW_9O_{34}]\cdot 7H_2O$ ({PW_9}) promoted the reaction; however, $ThCl_4$ afforded a significantly higher yield than {PW_9}, indicating that Th^{4+} plays a dominant role in the catalytic process. Moreover, a physical

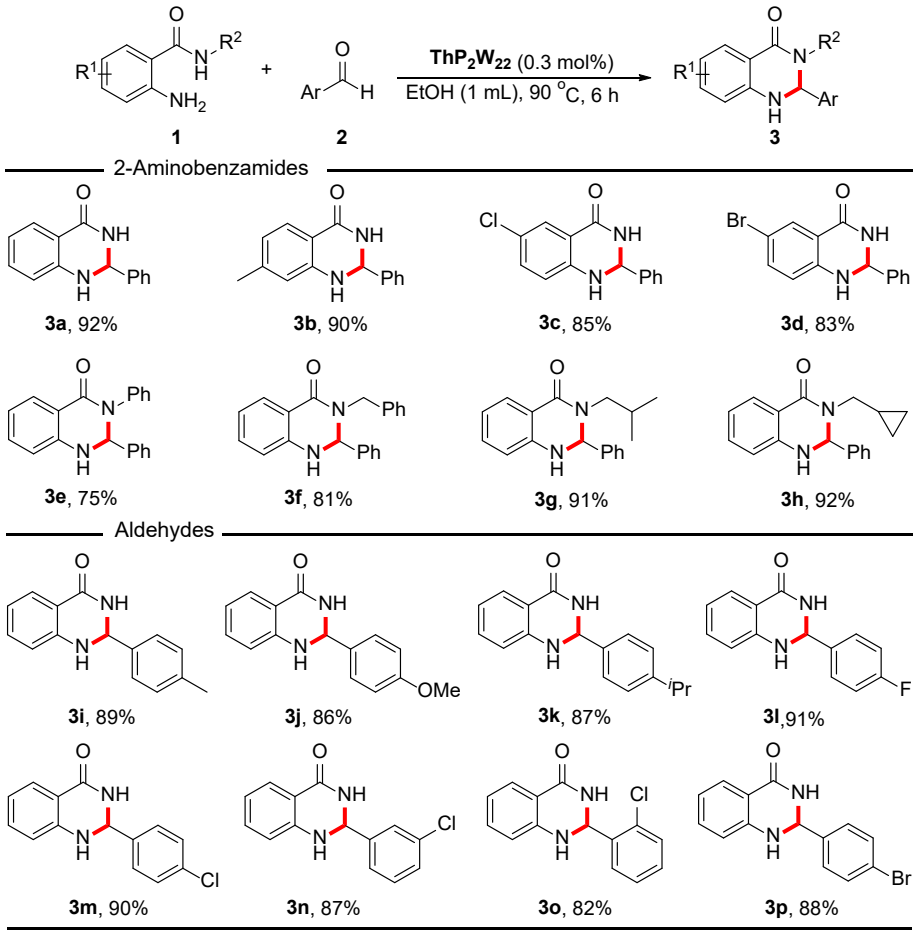

Figure 2 Universality of the ThP_2W_{22}-catalyzed reaction.

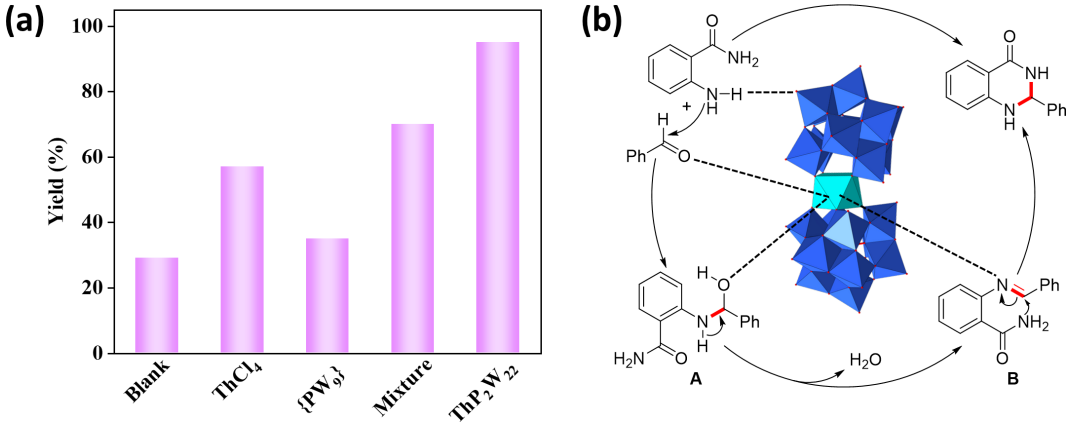

Figure 3 (a) Control experiments. (b) The possible mechanism.

mixture of $ThCl_4$ and $\{PW_9\}$ exhibited higher activity than either component alone but lower activity than $\mathbf{ThP_2W_{22}}$. These observations suggest a synergistic interaction between Th^{4+} and the $\{PW_9\}$ framework, and that integration within a defined crystal structure enhances catalytic efficiency. On the basis of these results and relevant literature, a plausible mechanism is proposed (Fig. 3(b)). The Th^{4+} center in $\mathbf{ThP_2W_{22}}$ functions as a Lewis acid, activating the aldehyde carbonyl group toward nucleophilic attack. Simultaneously, the oxygen-rich polyanionic surface may interact with the amine substrate through hydrogen bonding (N–H···O), facilitating substrate organization and increasing local concentration. This cooperative activation promotes formation of the aldimine intermediate, which subsequently undergoes intramolecular cyclization to afford the desired product **3a**.

4 Conclusions

In summary, a novel Th-containing phosphotungstate ($\mathbf{ThP_2W_{22}}$), constructed from two monolacunary Keggin-type units bridged by a Th^{4+} center formed *in situ*, was successfully synthesized and characterized. $\mathbf{ThP_2W_{22}}$ represents a rare example of a sandwich-type Th–phosphotungstate hybrid. Its successful preparation

addresses the challenge of incorporating thorium into POM frameworks and expands the structural diversity of actinide-containing clusters. Moreover, $\mathbf{ThP_2W_{22}}$ functions as an efficient Lewis acid catalyst for the synthesis of biologically relevant 2,3-dihydroquinazolinones under mild and green reaction conditions, exhibiting broad substrate scope. This work provides new insights into the design and application of Th-containing POMs.

Electronic Supplementary Material: Supplementary material (crystal data, bond valence calculations, structural figures, FT-IR spectra, TGA curves, PXRD patterns, and GC-MS spectra) is available in the online version of this article at https://doi.org/10.26599/POM.2026.9140121.

Data availability

All data needed to support the conclusions in the paper are presented in the manuscript and the Electronic Supplementary Material. Additional data related to this paper may be requested from the corresponding author upon request.

Acknowledgements

This work was supported by the National Natural Science Foundation of China (No. 22371040) and Jiangxi Provincial Natural Science Foundation (No. 20232ACB213005).

Declaration of competing interest

All the contributing authors report no conflict of interests in this work.

Author contribution statement

X. J. C.: Data curation, validation, experimental design. F. H. Z.: Data curation, validation. J. W. C.: writing manuscript. Z. B. Z.: Project administration. G. P. Y.: Project administration, funding acquisition, writing manuscript. All the authors have approved the final manuscript.

Use of AI statement

None.

References

[1] Li, H. F.; Yang, M. N.; Yuan, Z. L.; Sun, Y. H.; Ma, P. T.; Niu, J. Y.; Wang, J. P. Construction of one Ru_2W_{12}-cluster and six lacunary Keggin tungstoarsenate leading to the larger Ru-containing polyoxometalate photocatalyst. *Chin. Chem. Lett.* **2022**, *33*, 4664–4668.

[2] Liu, L. L.; Wang, L.; Xiao, X. Y.; Yang, P.; Zhao, J. W.; Kortz, U. Structural overview and evolution paths of lacunary polyoxometalates. *Coord. Chem. Rev.* **2024**, *506*, 215687.

[3] Liu, Y. F.; Hu, Q. L.; Chen, X. J.; Li, K.; Luo, P.; Yang, G. P. Two sandwich-type uranyl-containing polytungstates catalyze aerobic synthesis of benzimidazoles. *Rare Met.* **2024**, *43*, 1316–1322.

[4] Cai, Q. M.; Gao, R. L.; Wang, Y. F.; Xing, J. S.; Zhang, Q. Y.; Zhu, M. Z.; Qin, X. Y.; Liao, M. H.; Huang, Y. C. Ruthenium containing polyoxometalates: From synthesis, structures, properties to functional applications. *Polyoxometalates* **2025**, *4*, 9140083.

[5] Dong, Y. Y.; Hao, J. H.; Wang, Y. C.; Cao, X. H.; Dong, Z. M.; Zhang, Z. B.; Liu, Y. H. Recent advances in polyoxometalate-based functional materials for sustainable remediation of radionuclide and heavy metal pollution. *Chin. Chem. Lett.* **2025**, 111564.

[6] Li, S. R.; Liu, W. D.; Long, L. S.; Zheng, L. S.; Kong, X. J. Recent advances in polyoxometalate-based lanthanide-oxo clusters. *Polyoxometalates* **2023**, *2*, 9140022.

[7] Zhao, Z. C.; Wei, J. Y.; Lang, Z. L.; Chi, M. Z.; Liu, X. Y.; Yang, J. X.; Yang, G. Y.; Lv, H. J. A superatomic $\{Ag_8\}^{6+}$ cluster induced by asymmetric mixed-addendum polyoxometalate. *J. Am. Chem. Soc.* **2025**, *147*, 25107–25114.

[8] Huang, X. Q.; Liu, S.; Liu, G.; Tao, Y. W.; Wang, C. R.; Zhang, Y. L.; Li, Z.; Wang, H. W.; Zhou, Z.; Shen, G. D. et al. An unprecedented 2-fold interpenetrated *lvt* open framework built from Zn_6 ring seamed trivacant polyoxotungstates used for photocatalytic synthesis of pyridine derivatives. *Appl. Catal. B: Environ.* **2023**, *323*, 122134.

[9] Cao, J. W.; Jiao, L. Y.; Zhang, F. H.; Wang, H. Z.; Xia, W. Q.; Cao, X. H.; Yang, G. P. Dual-ligand-regulated Tb-containing antimonotungstate for the heterogeneous catalytic synthesis of N-heterocycles in ethanol. *Inorg. Chem.* **2025**, *64*, 13157–13162.

[10] Gong, T. T.; Chen, Y. N.; Wang, S.; Wang, M.; Zhao, J. W. Rigid-flexible-ligand-ornamented lanthanide-incorporated selenotungstates and photoluminescence properties. *Chin. J. Struct. Chem.* **2024**, *43*, 100370.

[11] Li, H. L.; Lian, C.; Yang, G. Y. A new 4-Ti-added polyoxometalate. *Tungsten* **2024**, *6*, 465–471.

[12] Liu, W. D.; Zhu, H. T.; Zhang, X.; Su, F.; Sang, X. J.; Zhang, X. L.; Zhang, L. C. Room temperature self-assembly and nonenzymatic electrochemical sensing performance of transition metal-embedded wheel-shaped tungstophosphates. *Polyoxometalates* **2025**, *4*, 9140073.

[13] Zhang, X. Y.; Li, H.; Xu, N.; Liu, X. D.; Wang, X. L. Engineering geometric metamorphosis in $\{P_6M_2Mo_{16}O_{73}\}$-based high-nuclearity metal superclusters: From tetrahedral to square assemblies via topological transformations. *Inorg. Chem. Front.* **2025**, *12*, 3823–3832.

[14] Zhou, D. X.; Li, B. B.; Zhao, Q. X.; Tang, X. Y.; Lan, T. Y.; Su, H. Y.; Yang, G. P.; Xuan, W. M. Solvent-modulated assembly of peptide and cerium functionalized gigantic $\{Mo_{120}Ce_6\}_2$ dimers for high-efficiency photocatalytic oxidation. *Inorg. Chem. Front.* **2024**, *11*, 2355–2364.

[15] Auvray, T.; Matson, E. M. Polyoxometalate-based complexes as ligands for the study of actinide chemistry. *Dalton Trans.* **2020**, *49*, 13917–13927.

[16] Colla, C. A.; Colliard, I.; Sawvel, A. M.; Nyman, M.; Mason, H. E.; Deblonde, G. J. P. Contrasting trivalent lanthanide and actinide complexation by polyoxometalates via solution-state NMR. *Inorg. Chem.* **2023**, *62*, 6242–6254.

[17] Colliard, I.; Deblonde, G. J. P. Polyoxometalate ligands reveal different coordination chemistries among lanthanides and heavy actinides. *JACS Au* **2024**, *4*, 2503–2513.

[18] Dufaye, M.; Duval, S.; Loiseau, T. Trends and new directions in the crystal chemistry of actinide oxo-clusters incorporated in polyoxometalates. *CrystEngComm* **2020**, *22*, 3549–3562.

[19] Kim, K. C.; Pope, M. T. Cation-directed structure changes in polyoxometalate chemistry. Equilibria between isomers of bis(9-tungstophosphatodioxouranate(VI)) complexes. *J. Am. Chem. Soc.* **1999**, *121*, 8512–8517.

[20] Yang, G. P.; Li, K.; Hu, C. W. Recent advances in uranium-containing polyoxometalates. *Inorg. Chem. Front.* **2022**, *9*, 5408–5433.

[21] Tamain, C.; Dumas, T.; Hennig, C.; Guilbaud, P. Coordination of tetravalent actinides (An = Th^{IV}, U^{IV}, Np^{IV}, Pu^{IV}) with DOTA: From dimers to hexamers. *Chem.—Eur. J.* **2017**, *23*, 6864–6875.

[22] Tutson, C. D.; Gorden, A. E. V. Thorium coordination: A comprehensive review based on coordination number. *Coord. Chem. Rev.* **2017**, *333*, 27–43.

[23] Xiao, B.; Gesing, T. M.; Robben, L.; Bosbach, D.; Alekseev, E. V. Dinuclear face-sharing bi-octahedral tungsten(VI) core and unusual

thermal behavior in complex Th tungstates. *Chem.—Eur. J.* **2015**, *21*, 7746–7754.
[24] Niu, Q.; Huang, Q.; Yu, T. Y.; Liu, J.; Shi, J. W.; Dong, L. Z.; Li, S. L.; Lan, Y. Q. Achieving high photo/thermocatalytic product selectivity and conversion via thorium clusters with switchable functional ligands. *J. Am. Chem. Soc.* **2022**, *144*, 18586–18594.
[25] Colliard, I.; Brown, J. C.; Nyman, M. Metal-oxo cluster formation using ammonium and sulfate to differentiate M^{IV} (Th, U, Ce) chemistries. *Inorg. Chem.* **2023**, *62*, 1891–1900.
[26] Falaise, C.; Kozma, K.; Nyman, M. Thorium oxo-clusters as building blocks for open frameworks. *Chem.—Eur. J.* **2018**, *24*, 14226–14232.
[27] Knope, K. E.; Vasiliu, M.; Dixon, D. A.; Soderholm, L. Thorium(IV)-selenate clusters containing an octanuclear Th(IV) hydroxide/oxide core. *Inorg. Chem.* **2012**, *51*, 4239–4249.
[28] Lin, J.; Jin, G. B.; Soderholm, L. $Th_3[Th_6(OH)_4O_4(H_2O)_6](SO_4)_{12}(H_2O)_{13}$: A self-assembled microporous open-framework thorium sulfate. *Inorg. Chem.* **2016**, *55*, 10098–10101.
[29] Chiang, M. H.; Williams, C. W.; Soderholm, L.; Antonio, M. R. Coordination of actinide ions in wells-dawson heteropolyoxoanion complexes. *Eur. J. Inorg. Chem.* **2003**, *2003*, 2663–2669.
[30] Duval, S.; Béghin, S.; Falaise, C.; Trivelli, X.; Rabu, P.; Loiseau, T. Stabilization of tetravalent 4f (Ce), 5d (Hf), or 5f (Th, U) clusters by the $[\alpha\text{-}SiW_9O_{34}]^{10-}$ polyoxometalate. *Inorg. Chem.* **2015**, *54*, 8271–8280.
[31] >Griffith, W. P.; Morley-Smith, N.; Nogueira, H. I. S.; Shoair, A. G. F.; Suriaatmaja, M.; White, A. J. P.; Williams, D. J. Studies on polyoxo and polyperoxo-metalates: Part 7. Lanthano- and thoriopolyoxotungstates as catalytic oxidants with H_2O_2 and the X-ray crystal structure of $Na_8[ThW_{10}O_{36}]\cdot 28H_2O$. *J. Organomet. Chem.* **2000**, *607*, 146–155.
[32] Ostuni, A.; Bachman, R. E.; Pope, M. T. Multiple diastereomers of $[Mn^{+}(\alpha_m\text{-}P_2W_{17}O_{61})_2]^{(20-n)-}$ (M = U^{IV}, Th^{IV}, Ce^{III}; m = 1, 2). Syn- and anti-conformations of the polytungstate ligands in $\alpha_1\alpha_1$, $\alpha_1\alpha_2$, and $\alpha_2\alpha_2$ complexes. *J. Cluster Sci.* **2003**, *14*, 431–446.
[33] Dufaye, M.; Duval, S.; Stoclet, G.; Loiseau, T. Crystal chemistry and SAXS studies of an octahedral polyoxoarsenotungstate nanocluster encapsulating four unprecedented thorium arsenate fragments ($\{Th_3As_2O_n\}$ - n = 25 or 26). *Eur. J. Inorg. Chem.* **2019**, *2019*, 4500–4505.
[34] Chinigo, G. M.; Paige, M.; Grindrod, S.; Hamel, E.; Dakshanamurthy, S.; Chruszcz, M.; Minor, W.; Brown, M. L. Asymmetric synthesis of 2, 3-dihydro-2-arylquinazolin-4-ones: Methodology and application to a potent fluorescent tubulin inhibitor with anticancer activity. *J. Med. Chem.* **2008**, *51*, 4620–4631.
[35] Jiao, J. J.; Li, Z. J.; Qiao, Z. W.; Li, X.; Liu, Y.; Dong, J. Q.; Jiang, J. W.; Cui, Y. Design and self-assembly of hexahedral coordination cages for cascade reactions. *Nat. Commun.* **2018**, *9*, 4423.
[36] Xing, Z. M.; Wu, W. H.; Miao, Y. X.; Tang, Y. Q.; Zhou, Y. K.; Zheng, L. F.; Fu, Y.; Song, Z. B.; Peng, Y. Y. Recent advances in quinazolinones as an emerging molecular platform for luminescent materials and bioimaging. *Org. Chem. Front.* **2021**, *8*, 1867–1889.
[37] Borah, B.; Swain, S.; Patat, M.; Chowhan, L. R. Recent advances and prospects in the organocatalytic synthesis of quinazolinones. *Front. Chem.* **2022**, *10*, 991026.
[38] Kumar, G.; Mogha, N. K.; Masram, D. T. Zr-based metal-organic framework/reduced graphene oxide composites for catalytic synthesis of 2, 3-dihydroquinazolin-4(1*H*)-one derivatives. *ACS Appl. Nano Mater.* **2021**, *4*, 2682–2693.
[39] Li, K.; Liu, Y. F.; Yang, G. P.; Zheng, Z. J.; Lin, X. L.; Zhang, Z. B.; Li, S. J.; Liu, Y. H.; Wei, Y. G. Highly-stable Silverton-type U^{IV}-containing polyoxomolybdate frameworks for the heterogeneous catalytic synthesis of quinazolinones. *Green Chem.* **2024**, *26*, 6454–6460.
[40] Yang, G. P.; Cao, J. W.; Lin, Z. F.; Li, S. X.; Dong, Y. Y.; Liu, Y. F. Praseodymium-selenium connecting selenotungstate containing mixed building blocks for catalytic synthesis of aza-heterocycles. *Inorg. Chem. Front.* **2025**, *12*, 1831–1838.

Zhibin Zhang received his B. S. degree from East China University of Technology in 2004, his Ph.D. degree from Nanjing Tech University in 2009. He is currently a professor at East China University of Technology. His research focuses on the separation, enrichment, and nuclear waste treatment of radionuclides.

Guoping Yang received his B. S. degree from Changzhi University in 2011, his M. S. degree from Guangxi Normal University in 2014, and his Ph.D. degree from Beijing Institute of Technology in 2019. He is currently an associate researcher at the Jiangxi Key Laboratory for Mass Spectrometry and Instrumentation, East China University of Technology. He focuses his research on the design and assembly of novel actinide crystalline materials (MOFs/POMs), green catalytic organic synthesis, and photocatalytic chemistry.